Accurate Computational Algorithm for Calculation of Input Impedance of Antennas of Arbitrarily Shaped Conducting Surfaces

Khalid F. A. Hussein

Microwave Eng. Dept., Electronics Research Inst., Dokki, Cairo, Egypt

Abstract **–** In the present work, a Galerkin's electric field integral equation (EFIE) solution is applied to get the current flowing on a conducting surface of arbitrary shape when excited by a gap generator as well as when illuminated by an incident plane wave. The main objective of this work is to get a fast, accurate and efficient computer algorithm that optimizes the use of computer resources and reduces the computational time and to accurately evaluate the input impedance of conducting surface antennas. The singular integrals arising in such a Galerkin's formulation are accurately evaluated and obtained as analytic expressions. An efficient method is described for accurate evaluation of the input impedance for antennas of arbitrarily-shaped conducting surface. The efficiency of the applied Galerkin's algorithm is examined by calculating the input impedance of well known antennas of conducting surfaces such as the strip-dipole, bow-tie and planar equiangular spiral antennas. To investigate the accuracy of the applied technique the results concerning these antennas are presented and compared with some published results.

I. INTRODUCTION

Among the electromagnetic techniques used for treating the problems of scattering, antennas and discontinuities in waveguides, the integral equation is one of the most widely used techniques. In electromagnetic integral equation methods, the original boundary value problems for Maxwell equations are reformulated as integral equations over the boundary interfaces of homogeneous domains. If the object is inhomogeneous, integral equation over the entire volume of the object has to be considered.

One of the most powerful techniques used in the electromagnetic modeling of conducting bodies is based on the EFIE formulation of the Maxwell equations [1 - 7]. The EFIE solution for scattering from conducting surfaces of arbitrary shape was developed by Rao, Wilton and Glisson (RWG) in [8]. In the same paper, triangular basis functions, commonly known as RWG basis functions, were introduced for current expansion on the conducting surface. Since that time, this formulation of EFIE together with the triangular-patch surface modeling have become one of the most widely used techniques for solving electromagnetic scattering and radiation problems.

A point-matching method of moments (MoM) solution was applied in [8] to get the current on an arbitrary surface. This technique ensures the satisfaction of the boundary conditions (that yield the vanishing of the tangential electric field on the conducting surface) at the centroids of the triangular patches forming the conducting surface. However, residual errors remain at the other points of the surface.

In [9] and [10], the problems that arise when a Galerkin technique is applied for the formulation and solution of the EFIE for conducting surfaces are treated. Their main purpose was to evaluate accurately the singular integrals arising in such a Galerkin formulation rather than the description of a computational algorithm for the application of Galerkin's technique on an arbitrarily shaped conducting surface.

In the present work, the Galerkin solution is applied to the EFIE to get the current flowing on the conducting body surface in a way to get a complete description of a fast, accurate and efficient algorithm that optimizes the use of computer resources and reduces the computational time.

The singular integrals encountered when Galerkin's formulation is used are classified and evaluated analytically. The integrals involved are carried out on planar triangular patches and, hence, they can be evaluated by first transforming from the 3D Cartesian coordinates to the so-called simplex coordinates. The analytic expressions for the singular integrals provided in [11] are used here to accurately evaluate the singular integrals.

Three types of singular integrals appear in Galerkin's formulation. The first type results when the source and observation triangular patches are the same. The second type results when the two patches share a

common edge. The third type of such singular integrals results when the source and observation patches share a common vertex. These singular integrals are reduced to a standard form, which is evaluated analytically by the expressions provided in [11].

An efficient method is described for accurate evaluation of the input impedance for antennas of arbitrarily-shaped conducting surface. The efficiency of the applied Galerkin's algorithm is examined by calculating the input impedance of well known antennas of conducting surfaces such as the strip-dipole, bow-tie and planar equiangular spiral antennas. To investigate the accuracy of the applied technique the results concerning these antennas are presented and compared with some published results.

It may be worth noting that the characteristics of a conical equiangular spiral antenna were investigated in [12] using the EFIE. However, the work of [12] employs a point matching technique and not a Galerkin's one, which arrives at different singular integrals. The method presented here (section 5) for evaluating the input impedance was not included in [12]. Furthermore, the present work uses a method of calculating the singular integrals, which is more accurate than that used in [12].

II. FORMULATION OF GALERKIN'S EFIE

It is required to deduce the current flowing on a conducting surface due to an exciting source, which may be an incident wave or a generator attached to the conducting surface. The formulation of the EFIE that is to be solved for the current distribution on the conducting surface requires, first, modeling the scatterer or antenna surface by triangular patches. Then, the linear density of the current on the surface is expanded using the appropriate basis functions with unknown amplitudes. A Galerkin's testing procedure is then applied to get the unknown amplitudes.

A. Modeling the Surface of the Scatterer

As shown in Fig. 1-a, the surface is divided into a number of triangular patches. Each patch has three edges; an edge which belongs to only one triangular patch is called a *boundary edge*. Such an edge exists only on the rim of an open surface and hence, it has no electric current component flowing normal to it. As shown in Fig. 1-b, an edge which belongs to two adjacent triangular patches is called a *non-boundary edge*. Only non-boundary edges can have electric current components flowing normal to them.

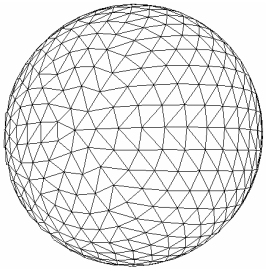

(a) Triangular-patch Model.

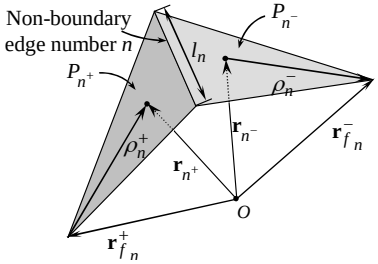

(b) Two triangular patches sharing an edge.

Fig. 1. Triangular-patch model for surfaces of arbitrarily-shaped scatterers and antennas.

Let the number of the triangular patches constituting the surface model be Q and the number of the non-boundary edges be N. Let P_q denote the triangular patch whose index (number) is q; q = 0,1,2,……Q-1. Two adjacent triangular patches P_{n^+} and P_{n^-} sharing the edge number n are shown in Fig. 1-b, where n^+ and n^- are, respectively, the patch indices. It should be noted that both the values of n^+ and n^- have no relation to the value of n. This notation is used only to indicate that the triangular patches whose indices are $q=n^+$ and $q=n^-$ are adjacent patches and share the edge number n, with a plus or minus designation determined by the choice of a positive current reference direction for the shared edge number n. This direction is assumed to be from P_{n^+} to P_{n^-}. That is, n^+ is the number of the patch of which the current component associating the edge number n is assumed to be flowing out, whereas n^- is the number of the patch into which this current is flowing. This means that n^+=1,2,3,…..,Q and n^-=1,2,3,…,Q whereas n=1,2,3,…..,N. A point in P_{n^+} can be specified by the position vector $\mathbf{r}_{n^+}$ defined with respect to the origin O, or by the position vector $\boldsymbol{\rho}_n^+$ defined with respect to the free vertex, $\mathbf{r}_{f\,n}^+$, of the triangular facet P_{n^+} (*i.e.* the vertex of P_{n^+} which does not belong to P_{n^-}). Similarly,

a point in P_{n^-} can be specified by $\mathbf{r}_{n^-}$ or $\boldsymbol{\rho}_n^-$. It should be noticed that the position vector $\boldsymbol{\rho}_n^+$ is directed from the free vertex, $\mathbf{r}_{f\,n}^+$, of P_{n^+} toward the point in the patch whereas the position vector $\boldsymbol{\rho}_n^-$ is directed from the point to the free vertex, $\mathbf{r}_{f\,n}^-$, of P_{n^-}. Thus one can write,

$$\boldsymbol{\rho}_n^{\pm} = \pm\,(\mathbf{r}_{n^{\pm}} - \mathbf{r}_{f\,n}^{\pm})\,. \tag{1}$$

B. Representation of the Current on the Scatterer

The current flowing on the conducting surface is expressed as a summation of vector basis functions with unknown amplitudes. The most suitable basis function for describing the current flowing on the triangular patches used for modeling the conducting surface is the Rao-Wilton-Glisson basis function given in [8]. For each non-boundary edge, a vector basis function is defined as follows,

$$\mathbf{f}_n(\mathbf{r}) = \begin{cases} \dfrac{l_n}{2S_{n^+}}\boldsymbol{\rho}_n^+, & \mathbf{r}\in P_{n^+} \\ \dfrac{l_n}{2S_{n^-}}\boldsymbol{\rho}_n^-, & \mathbf{r}\in P_{n^-} \\ 0, & \text{otherwise} \end{cases} \tag{2}$$

where l_n is the length of the non-boundary edge number n, S_{n^+} and S_{n^-} are the areas of the triangular patches P_{n^+} and P_{n^-}, respectively. It can be shown that the normal component of $f_n(r)$ at the n^{th} edge is unity [8]. Using the basis function $f_n(r)$, the linear current density on the conducting surface can be expressed as,

$$\mathbf{J} = \sum_{n=1}^{N} I_n \mathbf{f}_n(\mathbf{r}) \tag{3}$$

where I_n; n = 1,2,3…N are unknown amplitudes of the basis functions and to be determined by the following procedure.

C. Application of the Galerkin's Testing Procedure

The electric field radiated by a surface charge density σ and linear current density **J** flowing on a conducting surface, S, can be obtained by the following expression,

$$\mathbf{E}^s(\mathbf{r}) = -\,j\omega\mathbf{A}(\mathbf{r}) - \nabla\Phi(\mathbf{r}) \tag{4}$$

where $\mathbf{A}(\mathbf{r})$ is the vector magnetic potential defined as,

$$\mathbf{A}(\mathbf{r}) = \frac{\mu}{4\pi}\int_{S'} \mathbf{J}\,\frac{e^{-jk|\mathbf{r}-\mathbf{r}'|}}{|\mathbf{r}-\mathbf{r}'|}\,dS'\,, \tag{5}$$

and $\Phi(\mathbf{r})$ is the scalar electric potential defined as,

$$\Phi(\mathbf{r}) = \frac{1}{4\pi\varepsilon}\int_{S'} \sigma\,\frac{e^{-jk|\mathbf{r}-\mathbf{r}'|}}{|\mathbf{r}-\mathbf{r}'|}\,dS' \tag{6}$$

where $\mathbf{r}'$ is a point on S and $\mathbf{r}$ is a point in the near or far zone of free space. The surface charge density σ is related to the surface divergence of the current **J** flowing on S through the equation of continuity,

$$\nabla_s \cdot \mathbf{J} = -\,j\omega\sigma\,. \tag{7}$$

On the conducting surface, the tangential electric field must vanish yielding the following equation,

$$-\,\mathbf{E}_{tan}^i(\mathbf{r}) = -\,j\omega\mathbf{A}_{tan}(\mathbf{r}) - \nabla_s\Phi(\mathbf{r})\,. \tag{8}$$

Define the product

$$\langle \mathbf{a},\mathbf{b}\rangle = \int_S \mathbf{a}\cdot\mathbf{b}\;dS\,. \tag{9}$$

This product can be applied to (8) to get

$$\left\langle \mathbf{E}^i(\mathbf{r}),\mathbf{f}_m(\mathbf{r})\right\rangle = j\omega\left\langle \mathbf{A}(\mathbf{r}),\mathbf{f}_m(\mathbf{r})\right\rangle + \left\langle \nabla\Phi(\mathbf{r}),\mathbf{f}_m(\mathbf{r})\right\rangle \tag{10}$$

where the surface S in equation (9) is the combined area of the two patches sharing the non-boundary edge m. The product in the first term on the right-hand side of equation (10) can be expressed as,

$$\left\langle \mathbf{A}(\mathbf{r}),\mathbf{f}_m(\mathbf{r})\right\rangle = \int_{P_{m^+}} \mathbf{A}(\mathbf{r})\cdot\mathbf{f}_m(\mathbf{r})\,dS + \int_{P_{m^-}} \mathbf{A}(\mathbf{r})\cdot\mathbf{f}_m(\mathbf{r})\,dS\,. \tag{11}$$

The vector magnetic potential **A** can be expressed as the summation of its components which are attributed to the currents associating the non-boundary edges as follows,

$$\mathbf{A}(\mathbf{r}) = \sum_{n=1}^{N}\left[\mathbf{A}_{n^+}^n(\mathbf{r}) + \mathbf{A}_{n^-}^n(\mathbf{r})\right] \tag{12}$$

where $\mathbf{A}_{n^{\pm}}^n$ is the vector magnetic potential due to the current flowing through the patch $P_{n^{\pm}}$ and associated with the non-boundary edge n. Substituting equation (12) in equation (11), one gets

$$\left\langle \mathbf{A}(\mathbf{r}),\mathbf{f}_m(\mathbf{r})\right\rangle = \sum_{n=1}^{N}\left(A_{m^+n^+}^{mn} + A_{m^+n^-}^{mn} + A_{m^-n^+}^{mn} + A_{m^-n^-}^{mn}\right) \tag{13}$$

where

$$A_{m^{\pm}n^{\pm}}^{mn} = \int_{P_{m^{\pm}}} \mathbf{A}_{n^{\pm}}^n\cdot\mathbf{f}_m(\mathbf{r})\,dS\,. \tag{14}$$

According to equation (5), $\mathbf{A}_{n^{\pm}}^{n}$ can be expressed as

$$\mathbf{A}_{n^{\pm}}^{n}(\mathbf{r}) = \frac{\mu\, I_n}{4\pi} \int_{P_{n^{\pm}}} \mathbf{f}_n(\mathbf{r}')\ F_R\ dS' \tag{15}$$

where

$$F_R = \frac{e^{-jkR}}{R}. \tag{16}$$

Substituting equation (15) into equation (14), one gets

$$A_{m^{\pm}n^{\pm}}^{mn} = \frac{\mu\, I_n}{4\pi} \int_{P_{m^{\pm}}} \int_{P_{n^{\pm}}} \mathbf{f}_n(\mathbf{r}')\, F_R\ dS' \cdot \mathbf{f}_m(\mathbf{r})\, dS\,. \tag{17}$$

Substituting $\mathbf{f}_n(\mathbf{r}')$ and $\mathbf{f}_m(\mathbf{r})$ into equation (17), one gets

$$A_{m^{+}n^{+}}^{mn} = \frac{\mu\, I_n l_m l_n}{16\pi\, S_{m^{+}} S_{n^{+}}} \int_{P_{m^{+}}} \int_{P_{n^{+}}} F_R \boldsymbol{\rho}_n^{+} \cdot \boldsymbol{\rho}_m^{+} dS' dS\,, \tag{18-a}$$

$$A_{m^{+}n^{-}}^{mn} = \frac{\mu\, I_n l_m l_n}{16\pi\, S_{m^{+}} S_{n^{-}}} \int_{P_{m^{+}}} \int_{P_{n^{-}}} F_R \boldsymbol{\rho}_n^{-} \cdot \boldsymbol{\rho}_m^{+}\ dS' dS\,, \tag{18-b}$$

$$A_{m^{-}n^{+}}^{mn} = \frac{\mu\, I_n l_m l_n}{16\pi\, S_{m^{-}} S_{n^{+}}} \int_{P_{m^{-}}} \int_{P_{n^{+}}} F_R \boldsymbol{\rho}_n^{+} \cdot \boldsymbol{\rho}_m^{-} dS' dS\,, \tag{18-c}$$

$$A_{m^{-}n^{-}}^{mn} = \frac{\mu\, I_n l_m l_n}{16\pi\, S_{m^{-}} S_{n^{-}}} \int_{P_{m^{-}}} \int_{P_{n^{-}}} F_R \boldsymbol{\rho}_n^{-} \cdot \boldsymbol{\rho}_m^{-}\ dS' dS\,. \tag{18-d}$$

The product in the second term on the right-hand side of equation (10) can be expressed as follows [8],

$$\left\langle \nabla\Phi(\mathbf{r}), \mathbf{f}_m(\mathbf{r}) \right\rangle = \int_S \nabla\Phi(\mathbf{r}) \cdot \mathbf{f}_m(\mathbf{r})\, dS = -\int_S \Phi(\mathbf{r})\, \nabla_s \cdot \mathbf{f}_m(\mathbf{r})\, dS\,. \tag{19}$$

Taking S in equation (19) as the combined area of the triangular patches $P_{m^{+}}$ and $P_{m^{-}}$, equation (19) can be written as

$$\left\langle \nabla\Phi(\mathbf{r}), \mathbf{f}_m(\mathbf{r}) \right\rangle = -\int_{P_{m^{+}}} \Phi(\mathbf{r})\, \nabla_s \cdot \mathbf{f}_m(\mathbf{r})\, dS - \int_{P_{m^{-}}} \Phi(\mathbf{r})\, \nabla_s \cdot \mathbf{f}_m(\mathbf{r})\, dS\,. \tag{20}$$

The scalar potential Φ can be expressed as the summation of its components which are attributed to the currents associating the non-boundary edges as follows,

$$\Phi(\mathbf{r}) = \sum_{n=1}^{N} \left[\Phi_{n^{+}}(\mathbf{r}) + \Phi_{n^{-}}(\mathbf{r}) \right] \tag{21}$$

where $\Phi_{n^{\pm}}^{n}$ is the scalar potential due to the current flowing through the patch $P_{n^{\pm}}$ and associated with the non-boundary edge number n. Substituting equation (21) into equation (20), one gets,

$$\left\langle \nabla\Phi(\mathbf{r}), \mathbf{f}_m(\mathbf{r}) \right\rangle = \sum_{n=1}^{N} \left(\Phi_{m^{+}n^{+}}^{mn} + \Phi_{m^{+}n^{-}}^{mn} + \Phi_{m^{-}n^{+}}^{mn} + \Phi_{m^{-}n^{-}}^{mn} \right) \tag{22}$$

where

$$\Phi_{m^{\pm}n^{\pm}}^{mn} = \int_{P_{m^{\pm}}} \Phi_{n^{\pm}}^{n} \nabla_s \cdot \mathbf{f}_m(\mathbf{r})\, dS\,, \tag{23}$$

$$\Phi_{n^{\pm}}^{n}(\mathbf{r}) = -\frac{I_n}{4\pi\, j\, \omega\varepsilon} \int_{P_{n^{\pm}}} \nabla_s \cdot \mathbf{f}_n(\mathbf{r}')\ \frac{e^{-jkR}}{R}\ dS'\,, \tag{24}$$

$$\Phi_{m^{\pm}n^{\pm}}^{mn} = -\frac{I_n}{4\pi\, j\omega\varepsilon} \int_{P_{m^{\pm}}} \int_{P_{n^{\pm}}} \nabla_s \cdot \mathrm{f}_n(\mathrm{r}')\ \nabla_s \cdot\ \mathrm{f}_m(\mathrm{r}) F_R dS' dS. \tag{25}$$

Substituting $\mathbf{f}_n(\mathbf{r}')$ in equation (25), one gets the expressions,

$$\Phi_{m^{+}n^{+}}^{mn} = \frac{-I_n l_m l_n}{4\pi\ j\ \omega\varepsilon\ S_{m^{+}} S_{n^{+}}} \int_{P_{m^{+}}} \int_{P_{n^{+}}} F_R\ dS'\ dS\,, \tag{26-a}$$

$$\Phi_{m^{+}n^{-}}^{mn} = \frac{I_n l_m l_n}{4\pi\ j\ \omega\varepsilon\ S_{m^{+}} S_{n^{-}}} \int_{P_{m^{+}}} \int_{P_{n^{-}}} F_R\ dS'\ dS\,, \tag{26-b}$$

$$\Phi_{m^{-}n^{+}}^{mn} = \frac{I_n l_m l_n}{4\pi\ j\ \omega\varepsilon\ S_{m^{-}} S_{n^{+}}} \int_{P_{m^{-}}} \int_{P_{n^{+}}} F_R\ dS'\ dS\,, \tag{26-c}$$

$$\Phi_{m^{-}n^{-}}^{mn} = \frac{-I_n l_m l_n}{4\pi\ j\ \omega\varepsilon\ S_{m^{-}} S_{n^{-}}} \int_{P_{m^{-}}} \int_{P_{n^{-}}} F_R\ dS'\ dS\,. \tag{26-d}$$

Equation (13) can be rewritten as,

$$\left\langle \mathbf{A}(\mathbf{r}), \mathbf{f}_m(\mathbf{r}) \right\rangle = \sum_{n=1}^{N} \frac{\mu\, I_n}{4\pi} l_m l_n\ \alpha_{mn} \tag{27}$$

where

$$\alpha^{mn} = \alpha_{m^{+}n^{+}}^{mn} + \alpha_{m^{+}n^{-}}^{mn} + \alpha_{m^{-}n^{+}}^{mn} + \alpha_{m^{-}n^{-}}^{mn}\,, \tag{28}$$

$$\alpha_{m^{+}n^{+}}^{mn} = \frac{1}{4\, S_{m^{+}} S_{n^{+}}} \int_{P_{m^{+}}} \int_{P_{n^{+}}} \boldsymbol{\rho}_n^{+}\, F_R\ dS' \cdot \boldsymbol{\rho}_m^{+}\ dS\,, \tag{29-a}$$

$$\alpha_{m^{+}n^{-}}^{mn} = \frac{1}{4\, S_{m^{+}} S_{n^{-}}} \int_{P_{m^{+}}} \int_{P_{n^{-}}} \boldsymbol{\rho}_n^{-}\, F_R\ dS' \cdot \boldsymbol{\rho}_m^{+}\ dS\,, \tag{29-b}$$

$$\alpha_{m^{-}n^{+}}^{mn} = \frac{1}{4\, S_{m^{-}} S_{n^{+}}} \int_{P_{m^{-}}} \int_{P_{n^{+}}} \boldsymbol{\rho}_n^{+}\, F_R\ dS' \cdot \boldsymbol{\rho}_m^{-}\ dS\,, \tag{29-c}$$

$$\alpha_{m^{-}n^{-}}^{mn} = \frac{1}{4\, S_{m^{-}} S_{n^{-}}} \int_{P_{m^{-}}} \int_{P_{n^{-}}} \boldsymbol{\rho}_n^{-}\, F_R\ dS' \cdot \boldsymbol{\rho}_m^{-}\ dS\,. \tag{29-d}$$

Equation (20) can be written as,

$$\left\langle \nabla\Phi(\mathbf{r}), \mathbf{f}_m(\mathbf{r}) \right\rangle = \sum_{n=1}^{N} \frac{I_n}{\pi\ j\ \omega\varepsilon} l_m l_n\ \beta_{mn} \tag{30}$$

where,

$$\beta^{mn} = \beta^{mn}_{m^+n^+} + \beta^{mn}_{m^+n^-} + \beta^{mn}_{m^-n^+} + \beta^{mn}_{m^-n^-}, \quad (31)$$

$$\beta^{mn}_{m^+n^+} = \frac{1}{4\,S_{m^+}S_{n^+}} \int_{P_{m^+}} \int_{P_{n^+}} F_R \, dS' \, dS, \quad (32\text{-a})$$

$$\beta^{mn}_{m^+n^-} = \frac{1}{4\,S_{m^+}S_{n^-}} \int_{P_{m^+}} \int_{P_{n^-}} F_R \, dS' \, dS, \quad (32\text{-b})$$

$$\beta^{mn}_{m^-n^+} = \frac{1}{4\,S_{m^-}S_{n^+}} \int_{P_{m^-}} \int_{P_{n^+}} F_R \, dS' \, dS, \quad (32\text{-c})$$

$$\beta^{mn}_{m^-n^-} = \frac{1}{4\,S_{m^-}S_{n^-}} \int_{P_{m^-}} \int_{P_{n^-}} F_R \, dS' \, dS. \quad (32\text{-d})$$

The product in the left-hand side of equation (10) can be expressed as,

$$\left\langle \mathbf{E}^i(\mathbf{r}), \mathbf{f}_m(\mathbf{r}) \right\rangle = \frac{l_m}{2\,S_{m^+}} \int_{P_{m^+}} \mathbf{E}^i(\mathbf{r}) \cdot \boldsymbol{\rho}^+_m \, dS + \frac{l_m}{2\,S_{m^-}} \int_{P_{m^-}} \mathbf{E}^i(\mathbf{r}) \cdot \boldsymbol{\rho}^-_m \, dS. \quad (33)$$

Equation (33) can be written as,

$$\left\langle \mathbf{E}^i(\mathbf{r}), \mathbf{f}_m(\mathbf{r}) \right\rangle = V_m \quad (34)$$

where

$$V_m = l_m \, (v^m_{m^+} + v^m_{m^-}), \quad (35)$$

$$v^m_{m^\pm} = \frac{1}{2\,S_{m^\pm}} \int_{P_{m^\pm}} \mathbf{E}^i(\mathbf{r}) \cdot \boldsymbol{\rho}^\pm_m \, dS. \quad (36)$$

Making use of equations (27), (30) and (34), equation (10) yield,

$$\sum_{n=0}^{N-1} Z_{mn} \, I_n = V_m \quad (37)$$

where

$$Z_{mn} = l_m l_n \left(\frac{j\omega\mu}{4\pi} \alpha^{mn} + \frac{1}{\pi \, j\,\omega\varepsilon} \beta^{mn} \right). \quad (38)$$

Equation (37) can be written in a matrix form as,

$$[Z][I] = [V]. \quad (39)$$

The last matrix equation constitutes a linear system of *N* equations in *N* unknowns which are the amplitudes of the basis functions in the current expansion series of equation (3). It should be noticed that due to the Galerkin's formulation, the matrix [*Z*] is symmetric. The evaluation of the elements of [Z] requires the calculation of the integrals in equations (29) and (32), which are singular when the observation point coincides with the source point. The evaluation of such integrals requires, first, their transformation from the Cartesian coordinates to the so-called simplex coordinates.

III. TRANSFORMATION OF INTEGRALS TO SIMPLEX COORDINATES

The integrals in equations (29) and (32) are carried out on planar triangular patches, and hence, they can be evaluated by, first, transforming from ordinary 3-D Cartesian coordinates to the so-called simplex coordinate system, which is a 2-D coordinate system. Referring to Fig. 2, a point $\mathbf{r}_q$ that lies in the triangle whose vertices are described in the Cartesian coordinates as $\mathbf{r}_{1q}$, $\mathbf{r}_{2q}$, $\mathbf{r}_{3q}$ can be mapped to the simplex coordinate system to lie inside a standard triangle, shown in Fig. 3, defined by

$$(\eta, \xi): \quad 0 < \eta < 1, \quad 0 < \xi < (1 - \eta) \quad (40)$$

where the new coordinates are determined by,

$$\eta = \frac{S_1}{S_q}, \quad \xi = \frac{S_2}{S_q}. \quad (41)$$

Define a third coordinate ζ as,

$$\zeta = \frac{S_3}{S_q}. \quad (42)$$

Since $\frac{S_1}{S_q} + \frac{S_2}{S_q} + \frac{S_3}{S_q} = 1$, one gets,

$$\eta + \xi + \zeta = 1. \quad (43)$$

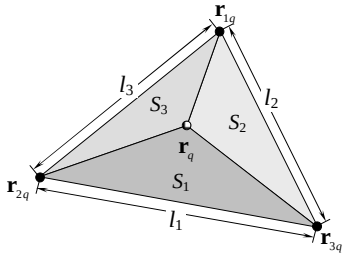

(a) Triangle in Cartesian coordinate system.

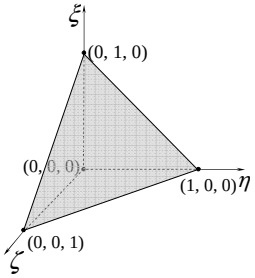

(b) The same triangle in simplex coordinate system.

Fig. 2. Transformation from Cartesian to simplex or normalized-area coordinates.

For this reason, the triplet (η, ξ ,ζ) describes the so-called normalized-area coordinate system shown in Fig. 2-b, which is equivalent to the simplex coordinate system (η, ζ) described by equations (40) and (41). Thus, a point r_q that lies in the triangular patch P_q and described in the simplex coordinate or normalized-area coordinate system as (η, ζ) or (η, ξ ,ζ) respectively, can be mapped to the 3D Cartesian coordinate system with the vertices $\mathbf{r_{1q}}$, $\mathbf{r_{2q}}$, $\mathbf{r_{3q}}$ of P_q using the transformation.

$$\mathbf{r}_q = \xi\ \mathbf{r}_{1q} + \eta\ \mathbf{r}_{2q} + (1 - \eta - \xi)\ \mathbf{r}_{3q} \tag{44}$$

or

$$\mathbf{r}_q = \eta\, \mathbf{r}_{1q} + \xi \mathbf{r}_{2q} + \zeta\, \mathbf{r}_{3q}\,. \tag{45}$$

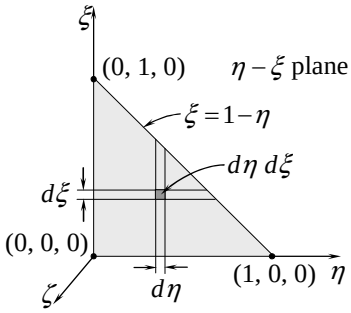

Fig. 3. Triangle transformed to simplex η-ξ plane.

It is required to express an infinitesimal element of area dS in terms of $d\eta$ and $d\xi$. Using η, ξ as 2D Cartesian-like coordinate as shown in Fig. 3, the triangular patch (of area S) is mapped to the right-angle triangle shown in the figure. If we express the area element in the η-ξ plane as $d\eta d\xi$, then integrating this element over the entire range of η, ξ results in the area of this triangle. To get the surface integrals in the η-ξ plane equivalent to the surface integrals in the ordinary 3D-Cartesian coordinates, the element $d\eta d\xi$ should be scaled; thus, we must have,

$$\int_0^1 \int_0^{1-\eta} S_f \ \ d\xi\, d\eta = S \tag{46}$$

where S_f is unknown scale factor that can be determined by carrying out the integration in equation(46). This leads,

$$S_f = 2S\,. \tag{47}$$

Thus, the surface integrals over P_q can be evaluated in the simplex coordinates by replacing dS by $2Sd\eta d\xi$, as follows,

$$\int_{P_q} g(\mathbf{r})\, dS\ = \ 2\, S_q \int_0^1 \int_0^{1-\eta} g[\xi\, \mathbf{r}_{1q} + \eta\, \mathbf{r}_{2q} + (1-\xi-\eta)\, \mathbf{r}_{3q}]\, d\xi d\eta\,. \tag{48}$$

Making use of equation (48), equations (29) and (32) can be written as,

$$\begin{aligned}\alpha_{m^{\pm}n^{\pm}}^{mn} = \pm \Big[& \mathbf{r}_{1m^{\pm}} \cdot \mathbf{r}_{1n^{\pm}}\ I_{\eta\eta'}^{m^{\pm}n^{\pm}} + \mathbf{r}_{2m^{\pm}} \cdot \mathbf{r}_{1n^{\pm}}\ I_{\xi\eta'}^{m^{\pm}n^{\pm}} \\ & + \mathbf{r}_{3m^{\pm}} \cdot \mathbf{r}_{1n^{\pm}}\ I_{\zeta\eta'}^{m^{\pm}n^{\pm}} - \mathbf{r}_{f\,m}^{\pm} \cdot \mathbf{r}_{1n^{\pm}}\ I_{\eta'}^{m^{\pm}n^{\pm}} \\ & + \mathbf{r}_{1m^{\pm}} \cdot \mathbf{r}_{2n^{\pm}}\ I_{\eta\xi'}^{m^{\pm}n^{\pm}} + \mathbf{r}_{2m^{\pm}} \cdot \mathbf{r}_{2n^{\pm}}\ I_{\xi\xi'}^{m^{\pm}n^{\pm}} \\ & + \mathbf{r}_{3m^{\pm}} \cdot \mathbf{r}_{2n^{\pm}}\ I_{\zeta\xi'}^{m^{\pm}n^{\pm}} - \mathbf{r}_{f\,m}^{\pm} \cdot \mathbf{r}_{2n^{\pm}}\ I_{\xi'}^{m^{\pm}n^{\pm}} \\ & + \mathbf{r}_{1m^{\pm}} \cdot \mathbf{r}_{3n^{\pm}}\ I_{\eta\zeta'}^{m^{\pm}n^{\pm}} + \mathbf{r}_{2m^{\pm}} \cdot \mathbf{r}_{3n^{\pm}}\ I_{\xi\zeta'}^{m^{\pm}n^{\pm}} \\ & + \mathbf{r}_{3m^{\pm}} \cdot \mathbf{r}_{3n^{\pm}}\ I_{\zeta\zeta'}^{m^{\pm}n^{\pm}} - \mathbf{r}_{f\,m}^{\pm} \cdot \mathbf{r}_{3n^{\pm}}\ I_{\zeta'}^{m^{\pm}n^{\pm}} \\ & - \mathbf{r}_{1m^{\pm}} \cdot \mathbf{r}_{f\,n}^{\pm}\ I_{\eta}^{m^{\pm}n^{\pm}} - \mathbf{r}_{2m^{\pm}} \cdot \mathbf{r}_{f\,n}^{\pm}\ I_{\xi}^{m^{\pm}n^{\pm}} \\ & - \mathbf{r}_{3m^{\pm}} \cdot \mathbf{r}_{f\,n}^{\pm}\ I_{\zeta}^{m^{\pm}n^{\pm}} + \mathbf{r}_{f\,m}^{\pm} \cdot \mathbf{r}_{f\,n}^{\pm}\ I^{m^{\pm}n^{\pm}} \Big], \end{aligned} \tag{49}$$

$$\beta_{m^{\pm}n^{\pm}}^{mn} = I^{m^{\pm}n^{\pm}}, \tag{50}$$

where

$$I_{\eta\eta'}^{pq} = \int_0^1 \int_0^{1-\eta} \int_0^1 \int_0^{1-\eta'} \eta\eta'\, F_R\, d\xi'\, d\eta'\, d\xi\, d\eta\,, \tag{51}$$

$$I_{\eta\xi'}^{pq} = \int_0^1 \int_0^{1-\eta} \int_0^1 \int_0^{1-\eta'} \eta\xi'\, F_R\, d\xi'\, d\eta'\, d\xi\, d\eta\,, \tag{52}$$

$$I_{\xi\eta'}^{pq} = \int_0^1 \int_0^{1-\eta} \int_0^1 \int_0^{1-\eta'} \xi\eta'\, F_R\, d\xi'\, d\eta'\, d\xi\, d\eta\,, \tag{53}$$

$$I_{\xi\xi'}^{pq} = \int_0^1 \int_0^{1-\eta} \xi \int_0^1 \int_0^{1-\eta'} \xi'\, F_R\, d\xi'\, d\eta'\, d\xi\, d\eta\,, \tag{54}$$

$$I_{\eta'}^{pq} = \int_0^1 \int_0^{1-\eta} \int_0^1 \int_0^{1-\eta'} \eta'\, F_R\, d\xi'\, d\eta'\, d\xi\, d\eta\,, \tag{55}$$

$$I_{\xi'}^{pq} = \int_0^1 \int_0^{1-\eta} \left(\int_0^1 \int_0^{1-\eta'} \xi'\, F_R\, d\xi'\, d\eta' \right) d\xi\, d\eta\,, \tag{56}$$

$$I_{\eta}^{pq} = \int_0^1 \int_0^{1-\eta} \eta \left(\int_0^1 \int_0^{1-\eta} F_R\, d\xi'\, d\eta' \right) d\xi\, d\eta\,, \tag{57}$$

$$I_{\xi}^{pq} = \int_0^1 \int_0^{1-\eta} \xi \left(\int_0^1 \int_0^{1-\eta} F_R\, d\xi'\, d\eta' \right) d\xi\, d\eta\,, \tag{58}$$

$$I^{pq} = \int_0^1 \int_0^{1-\eta} \left(\int_0^1 \int_0^{1-\eta'} F_R\, d\xi'\, d\eta' \right) d\xi\, d\eta \tag{59}$$

where $P = m^+, m^-$; $q = n^+, n^-$. The remaining integrals can be calculated from the above integrals as follows.

$$I_{\eta\zeta'}^{pq} = I_{\eta}^{pq} - I_{\eta\eta'}^{pq} - I_{\eta\xi'}^{pq}, \tag{60}$$

$$I_{\xi\zeta'}^{pq} = I_{\xi}^{pq} - I_{\xi\eta'}^{pq} - I_{\xi\xi'}^{pq}, \tag{61}$$

$$I^{pq}_{\zeta\eta'} = I^{pq}_{\eta'} - I^{pq}_{\eta\eta'} - I^{pq}_{\xi\eta'}, \quad (62)$$

$$I^{pq}_{\zeta\xi'} = I^{pq}_{\xi'} - I^{pq}_{\eta\xi'} - I^{pq}_{\xi\xi'}, \quad (63)$$

$$I^{pq}_{\zeta\zeta'} = I^{pq}_{\zeta'} - I^{pq}_{\eta\zeta'} - I^{pq}_{\xi\zeta'}, \quad (64)$$

$$I^{pq}_{\zeta'} = I^{pq} - I^{pq}_{\eta'} - I^{pq}_{\xi'}, \quad (65)$$

$$I^{pq}_{\zeta} = I^{pq} - I^{pq}_{\eta} - I^{pq}_{\xi}. \quad (66)$$

Thus, only nine independent integrals from equation (51) to equation (59) must be numerically evaluated for each combination of pairs; *p* and *q*. The nine integrals, in turn, contribute to up to nine elements of [*Z*] in equation (39). For a closed surface with *N* edges, the number of independent integrals computed is $4N^2$. By contrast, the edge-by-edge approach would require the evaluation of $36N^2$ integrals or nine times as many.

Due to the Galerkin's EFIE procedure applied as described above, and since the basis and testing functions chosen are identical, the *Z* matrix would then satisfy the symmetry property $Z_{mn}=Z_{nm}$. Also, the integrals in equation (51) to equation (66) are symmetric; i.e. $I^{pq}=I^{qp}$ and the same is true for the other integrals. Thus the number of the independent integrals that must be computed are reduced to $N(2N+3)$ instead of $4N^2$. Using the same coordinate transformation, equation (36) can be expressed as

$$v^m_{m^\pm} = \pm \int_0^1 \int_0^{1-\eta} \mathbf{E}^i(\mathbf{r}) \cdot \left| \xi \mathbf{r}_{1m^\pm} + \eta \mathbf{r}_{2m^\pm} + (1-\eta-\xi)\mathbf{r}_{3m^\pm} - \mathbf{r}^\pm_{f\,m} \right| d\xi\, d\eta. \quad (67)$$

Equation (67) can be written as,

$$v^m_{m^\pm} = \pm \left| \mathbf{r}_{1m^\pm} \cdot \mathbf{I}^{m^\pm}_\eta + \mathbf{r}_{2m^\pm} \cdot \mathbf{I}^{m^\pm}_\xi + \mathbf{r}_{3m^\pm} \cdot \mathbf{I}^{m^\pm}_\zeta - \mathbf{r}^\pm_{f\,m} \cdot \mathbf{I}^{m^\pm} \right| \quad (68)$$

where,

$$\mathbf{I}^p_\eta = \int_0^1 \int_0^{1-\eta} \eta \mathbf{E}^i[\xi \mathbf{r}_{1p} + \eta \mathbf{r}_{2p} + (1-\xi-\eta)\mathbf{r}_{3p}]\, d\xi\, d\eta, \quad (69)$$

$$\mathbf{I}^p_\xi = \int_0^1 \int_0^{1-\eta} \xi \mathbf{E}^i[\xi \mathbf{r}_{1p} + \eta \mathbf{r}_{2p} + (1-\xi-\eta)\mathbf{r}_{3p}]\, d\xi\, d\eta, \quad (70)$$

$$\mathbf{I}^p = \int_0^1 \int_0^{1-\eta} \mathbf{E}^i[\xi \mathbf{r}_{1p} + \eta \mathbf{r}_{2p} + (1-\xi-\eta)\mathbf{r}_{3p}]\, d\xi\, d\eta, \quad (71)$$

$$\mathbf{I}^p_\zeta = \mathbf{I}^p - \mathbf{I}^p_\eta - \mathbf{I}^p_\xi. \quad (72)$$

IV. EVALUATION OF SINGULAR INTEGRALS

Integrals of equation (51) to equation (59) are singular for *p=q i.e.*, when the source and observation patches are the same. In this case, each of these integrals can be divided into two parts one of which is non-singular and can be evaluated numerically whereas the other is weakly singular and can be evaluated analytically. The integral in equation (51) can be rewritten as,

$$I^{qq}_{\eta\eta'} = \int_0^1 \int_0^{1-\eta} \int_0^1 \int_0^{1-\eta'} \eta\eta' G_R \; d\xi'\, d\eta'\, d\xi\, d\eta + \Gamma^{qq}_{\eta\eta'} \quad (73)$$

where

$$G_R = \frac{e^{-jkR}-1}{R}, \quad (74)$$

$$\Gamma^{qq}_{\eta\eta'} = \int_0^1 \int_0^{1-\eta} \int_0^1 \int_0^{1-\eta'} \eta\eta' \frac{1}{R} \; d\xi'\, d\eta'\, d\xi\, d\eta. \quad (75)$$

It should be noted that the first term on the right hand side of equation (73) is a non-singular integral and can be evaluated numerically whereas $\Gamma^{qq}_{\eta\eta'}$ is weakly singular and should be evaluated analytically. The same can be repeated for equations (52) to (59), where these singular integrals appear,

$$\Gamma^{qq}_{\eta\eta'} = \int_0^1 \int_0^{1-\eta} \int_0^1 \int_0^{1-\eta'} \eta\eta' \frac{1}{R} \; d\xi'\, d\eta'\, d\xi\, d\eta, \quad (76)$$

$$\Gamma^{qq}_{\eta\xi'} = \int_0^1 \int_0^{1-\eta} \int_0^1 \int_0^{1-\eta'} \eta\xi' \frac{1}{R} \; d\xi'\, d\eta'\, d\xi\, d\eta, \quad (77)$$

$$\Gamma^{qq}_{\xi\eta'} = \int_0^1 \int_0^{1-\eta} \int_0^1 \int_0^{1-\eta'} \xi\eta' \frac{1}{R} \; d\xi'\, d\eta'\, d\xi\, d\eta, \quad (78)$$

$$\Gamma^{qq}_{\xi\xi'} = \int_0^1 \int_0^{1-\eta} \int_0^1 \int_0^{1-\eta'} \xi\xi' \frac{1}{R} \; d\xi'\, d\eta'\, d\xi\, d\eta, \quad (79)$$

$$\Gamma^{qq}_{\eta'} = \int_0^1 \int_0^{1-\eta} \int_0^1 \int_0^{1-\eta'} \eta' \frac{1}{R} \; d\xi'\, d\eta'\, d\xi\, d\eta, \quad (80)$$

$$\Gamma^{qq}_{\xi'} = \int_0^1 \int_0^{1-\eta} \int_0^1 \int_0^{1-\eta'} \xi' \frac{1}{R} \; d\xi'\, d\eta'\, d\xi\, d\eta, \quad (81)$$

$$\Gamma^{qq}_{\eta} = \int_0^1 \int_0^{1-\eta} \int_0^1 \int_0^{1-\eta'} \eta \frac{1}{R} \; d\xi'\, d\eta'\, d\xi\, d\eta, \quad (82)$$

$$\Gamma^{qq}_{\xi} = \int_0^1 \int_0^{1-\eta} \int_0^1 \int_0^{1-\eta'} \xi \frac{1}{R} \; d\xi'\, d\eta'\, d\xi\, d\eta, \quad (83)$$

$$\Gamma^{qq} = \int_0^1 \int_0^{1-\eta} \int_0^1 \int_0^{1-\eta'} \frac{1}{R} \; d\xi'\, d\eta'\, d\xi\, d\eta. \quad (84)$$

Closed form expressions for the singular integrals in equations (76) to (84) are given in Appendix A.

V. ANTENNA EXCITATION AND INPUT IMPEDANCE

In this section, a method is described for accurate computation of the input impedance of antennas composed of conducting surfaces using the EFIE technique.

For antennas composed of complex or curved conducting surfaces, the EFIE technique is preferable to the FDTD method [2]. The accuracy of the latter is often limited by the computer memory requirement and the "staircase" approximation of the antenna geometry. In antenna problems, the staircase approximation could become a major drawback for accurate impedance calculation since in this case very fine discretization of the antenna region near the feed point is required, which may be difficult for curved or complex surfaces. The EFIE technique employing triangular-patch model does not suffer from the staircase approximation and, moreover, the density of the triangular patches can be simply increased near the feeding point, as shown in Fig. 4, to get accurate evaluation of the impedance [13].

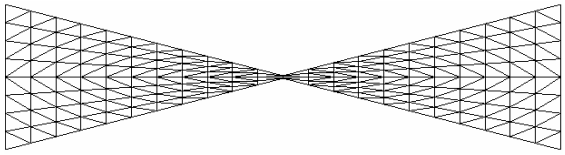

Fig. 4. Increasing the density of triangular patches near the feeding point of the antenna.

In scattering problems treated by the EFIE technique applied on a triangular-patch model of the scatterer, all the facets (triangular patches) are illuminated by the incident field. To excite an antenna by a delta-gap voltage generator, the delta gap is made as a cut along one or more of the non-boundary edges of the surface model. A voltage generator is then applied across the excitation edge(s). In this case, only the facets on the sides of each of the excitation edges have voltage difference applied on them. However, the method of evaluating the input impedance in the case of a conducting surface antenna excited by infinitesimal-gap voltage generator can be obtained from the model of scattering problem as detailed in the following analysis. Let m_x be the edge at which a delta-gap voltage source is applied and let m_x^+ and m_x^- be the numbers of triangular patches sharing this edge (the current is assumed to flow from m_x^+ to m_x^-). Consider the element number m_x in the excitation vector [V], which is expressed as,

$$\frac{V_{m_x}}{l_{m_x}} = \frac{1}{2S_{m_x^+}} \int_{P_{m_x^+}} \mathbf{E}^i \cdot \boldsymbol{\rho}_{m_x}^+ dS + \frac{1}{2S_{m_x^-}} \int_{P_{m_x^-}} \mathbf{E}^i \cdot \boldsymbol{\rho}_{m_x}^- dS \ . \quad (85)$$

For the purpose of physical interpretation of equation (85), this expression can be approximated as,

$$V_{m_x} / l_{m_x} \approx \mathbf{E}^i_{c\,m_x^+} \cdot \frac{\boldsymbol{\rho}_{c\,m_x}^+}{2} + \mathbf{E}^i_{c\,m_x^-} \cdot \frac{\boldsymbol{\rho}_{c\,m_x}^-}{2} \quad (86)$$

where, $E^i_{c\,m_x^+}$ and $E^i_{c\,m_x^-}$ are the values of the incident electric field at the centroids of the patches $P_{m_x^+}$ and $P_{m_x^-}$, respectively, and $\rho_{c\,m_x}^+$ and $\rho_{c\,m_x}^-$ are the position vectors of the centroids of the triangles $P_{m_x^+}$ and $P_{m_x^-}$ relative to the vertices $r_{f\,m_x}^+$ and $r_{f\,m_x}^-$, respectively. Thus, by the aid of Fig. 5, the quantity between square brackets in equation (86) can be interpreted as, approximately, the voltage difference between the centroids of the patches $P_{m_x^+}$ and $P_{m_x^-}$ or, in other words, the voltage drop across the excitation edge (*i.e.*, the voltage applied at the input port of the antenna). It should be noted that the value of V_{m_x} used in the present analysis is the exact one that is given by equation (85) and not equation (86). The purpose of obtaining the approximate expression is, only, to get a clear physical meaning of equation (85). According to equation (86), the voltage applied at the antenna input (*i.e.*, the voltage across the excitation edge) is expressed as,

$$V_{in} = V_{m_x} / l_{m_x} \ . \quad (87)$$

As discussed before, the coefficient I_{m_x} in the current expansion series is the normal component of the linear current density flowing past the edge m_x. Since this current density component is constant along the edge number m_x, the input current can be expressed as,

$$I_{in} = l_{m_x} I_{m_x} \ . \quad (88)$$

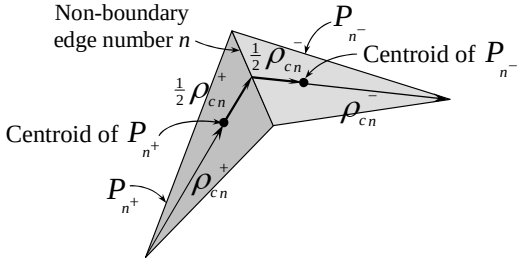

Fig. 5. The voltage drop across a non-boundary edge.

Using a triangular-patch model for the antenna, the input impedance can be defined as the voltage drop across the excitation edge, divided by the current flowing past this edge. Employing equations (87) and (88), one gets the following expression for the input impedance of the antenna,

$$Z_{in} = \frac{V_{in}}{I_{in}} = \frac{1}{l_{m_x}^2} \frac{V_{m_x}}{I_{m_x}}. \qquad (89)$$

It has been found that for an accurate calculation of input impedance, it is essential to use very fine discretization in the antenna region near the feed point. To reduce the number of unknowns, the region that is further away from the feed point can be descritized by less fine patches without essentially affecting accuracy. The mesh of a bow-tie antenna descritized with higher resolution in the region near the feeding point to get accurate value of the input impedance is shown in Fig. 4 [13].

VI. RESULTS AND DISCUSSION

The input impedance is one of the antenna parameters whose accuracy is strongly dependent on the efficiency of the computational technique through which it is evaluated. Hence, the evaluation of the antenna input impedance is one of the most stringent tests of the efficiency of a computational technique. Therefore the Galerkin's EFIE algorithm described in the present work is examined by its application to compute the input impedance of well-known conducting surface antennas such as the planar strip-dipole, bow-tie dipole and planar equiangular spiral antennas and comparing the obtained results with other published results concerning the same antennas.

A. Strip Dipole Antenna

The triangular-patch model for a straight strip-dipole antenna of length L and width W is shown in Fig. 6. A delta-gap generator of unity voltage is applied at the cut A-A'. The applied voltage is maintained constant along the feeding edge, which is the non-boundary edge at the center of the dipole. In this case, the input impedance can be obtained by calculating the current crossing the non-boundary edge A-A', and then employing equation (89).

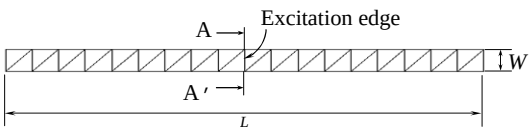

Fig. 6. Triangular patch model of a strip dipole antenna.

Figure 7 presents plots of the resistive and reactive components of the input impedance of a strip-dipole antenna against the operating frequency. The dipole length is 27 cm and its width is 0.001 of its length. The triangular-patch model of this antenna has 36 patches and 35 non-boundary edges. The results show agreement with those of [14]. Figure 8 shows a plot of the VSWR of the strip dipole with respect to 75 Ω source impedance against the frequency. It is clear in the Figure that the bandwidth of this antenna can be considered as 10%, a feature which is well-known for a half-wavelength straight dipole.

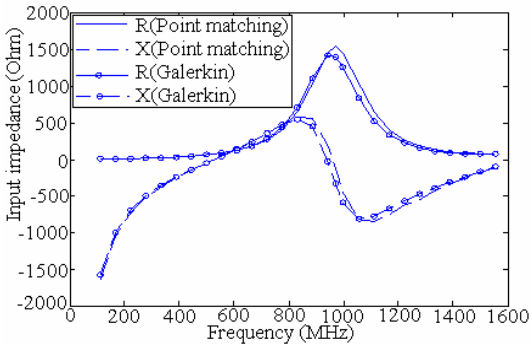

Fig. 7. Input Impedance of a planar strip dipole, L=27 cm and W= 2.7 mm.

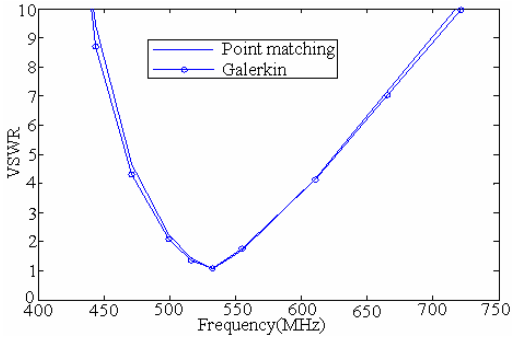

Fig. 8. VSWR of a planar strip dipole, L=27 cm, and W= 2.7 mm.

B. Bow-Tie Antenna

The main advantages of the bow-tie antenna are simple design and broad-band impedance. For this reason, a planar bow-tie antenna is used in many challenging recent applications such as ground penetrating radar (GPR) and global position system (GPS) applications and cellular-based mobile communication services [13], [14 - 20]. Figure 9 shows a triangular-patch model for a bow-tie antenna. The length of the antenna is 27 cm and the flare angle is 90º. The neck width of the antenna (length of the excitation edge) is 1.35 cm. The triangular-patch model of this antenna has 96 patches and 125 non-boundary edges. A delta-gap generator of unity voltage

is applied across the cut A-A', i.e. across the non-boundary edge at the center of the antenna. The current crossing this edge is calculated to get the input impedance via equation (89).

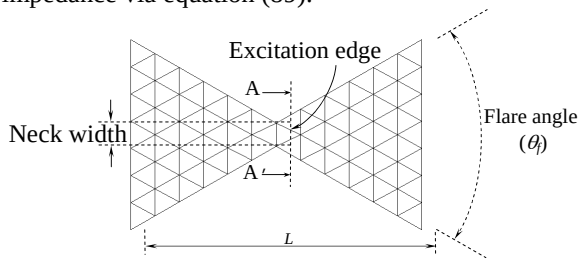

Fig. 9. Triangular patch model of a bow-tie antenna.

The dependence of the input impedance of a bow-tie antenna with the frequency is shown in Fig. 10. The results show good agreement with those of [16]. It should be noted that the antenna of the given dimensions is resonant at about 800 MHz where the input impedance is pure resistive. The VSWR of this antenna is plotted against the frequency as shown in Fig. 11, where the source impedance is assumed 300 Ω. It is clear in the figure that the bandwidth of the bow-tie antenna can be considered as about 400 MHz around its resonant frequency, *i.e.*, about 50%. Thus, the bow-tie antenna exhibits a much wider bandwidth than the dipole antenna, a feature which is well-established and is attributed to the fact that the width dimension of the bow-tie is described as an "angle" rather than a "length" but, however the bow-tie length is the dimensional parameter that limits the bandwidth of such an antenna.

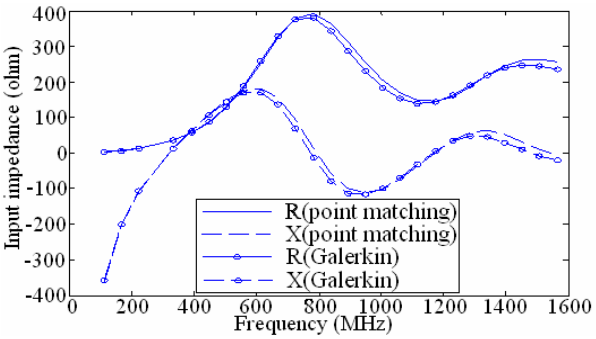

Fig. 10. Input Impedance of a bow-tie antenna, L=27 cm, and W= 1.35 cm, θ_f = 90°.

C. Planar Equiangular Spiral Antenna

One of the ultra wideband (UWB) antennas used in recent applications that require a well-suited transient antenna response is the planar equiangular spiral antenna. Due to its circular polarization, this antenna finds important applications such as short-pulse GPR systems that detect the objects buried in anisotropic ground. It also finds application in stepped-frequency GPR (SF-GPR) to detect buried non-metallic anti-personnel mines in humanitarian mine detection system [22]. Due to their characteristics of quite broad bandwidth and circular polarization, the spiral antennas are widely used in mobile-communication, early-warning and direction-finding systems [23]. The spiral antenna is also suitable as a wideband illuminator for a parabolic reflector working in ultra wideband of frequencies [24].

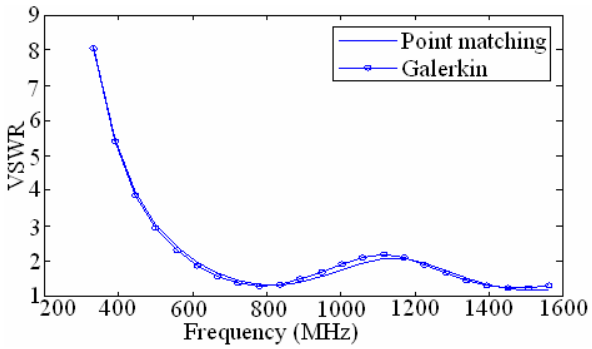

Fig. 11. VSWR for a bow-tie antenna, L=27 cm, and W=1.35cm, θ_f = 90°.

The radiation of spiral elements at the selected operating frequency comes from the active region where spiral circumference is approximately one wavelength. This means that the active region moves from the outermost circle to the innermost one as the frequency increases. Low frequency cutoff f_L is equal to $c/\pi D$ (c is the speed of light and D is the outermost diameter), but the upper frequency is determined by the feed point separation [20], [23] and [25].A triangular patch model for the equiangular spiral antenna surface model and the EFIE technique constitute the most efficient electromagnetic modeling of such an antenna. The triangular-patch model for this antenna is shown in Fig. 12.

Let us consider an equiangular spiral antenna of the following dimensions: the innermost diameter of the spiral (d) is 3 mm, the outermost diameter (D) is 29 cm, the wrapping angle (α) is 70° and the angular width of the spiral arm (δ) is 90°. The spiral arms are wound to make 4 complete revolutions. Figure 12-b shows the detailed triangular patch arrangement at the location of the antenna excitation. The triangular-patch model of this antenna has 138 patches and 177 non-boundary edges. A delta-gap generator of unity voltage slot generator is applied across the non-boundary edge at the cut A-A', where the voltage is maintained constant along this edge.

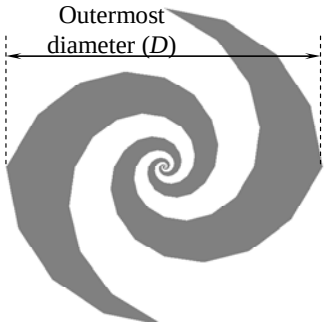

(a) Complete antenna.

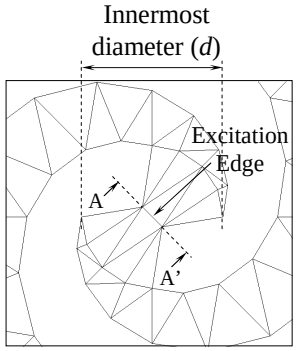

(b) Part of the antenna at the excitation.

Fig. 12. Triangular-patch model of an equiangular spiral antenna.

The input impedance is evaluated using equation (89). The variations of the resistive and reactive parts of the input impedance of the antenna described above with the frequency are presented in Fig. 13. It is clear that the input impedance is stable along a very wide range of the frequency; a fact that is well-known for such an antenna. The VSWR with respect to a source impedance of 150 Ω is plotted against the frequency as shown in Fig. 14. It is evident that this antenna is ultra-wideband; a feature which is attributed to the fact that the dimensions of such a spiral are mainly described as "angles" rather than "lengths".

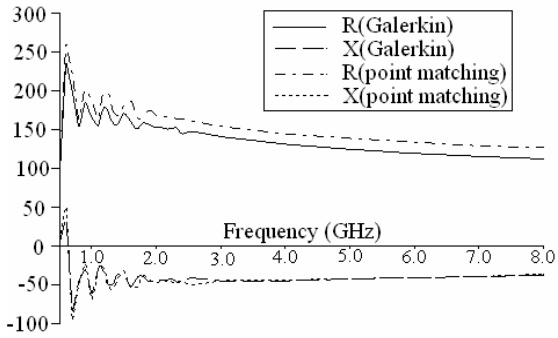

Fig. 13. Input Impedance of an equiangular spiral antenna, d = 3 mm, D = 29 cm, α = 70º and δ = 90º.

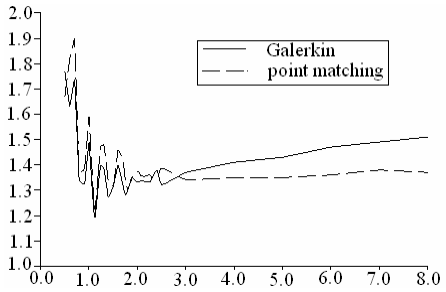

Fig. 14. VSWR of an equiangular spiral antenna, d = 3 mm, D = 29 cm, α = 70º and δ = 90º.

VII. CONCLUSION

A robust and efficient Galerkin's EFIE algorithm is developed to get the current distribution on arbitrarily-shaped conducting surface that act as scatterers or antennas. A new method is applied for accurate evaluation of the input impedance of antennas composed of conducting surfaces which are modeled by triangular patches when the antenna is excited by delta-gap voltage generator. The singular integrals arising when the source and observation points coincide are accurately evaluated. The efficiency of the algorithm is examined by calculating the input impedance and the VSWR of well-known types of antennas, where the results show good agreement with the already well-known characteristics of these antennas and are also in good agreement with some published results concerning the same antennas. The antennas examined in the present work are the strip-dipole, bow-tie and planar equiangular spiral antennas.

Appendix A: Analytic Evaluation of Singular Integrals

The following expressions for the singular integrals are given in [11] after making the corrections in [26],

$$\Gamma^{qq} = \frac{1}{6\sqrt{a}}(\gamma_2+\gamma_6)+\frac{1}{6\sqrt{c}}(\gamma_1+\gamma_5)+\frac{1}{6\sqrt{d}}(\gamma_3+\gamma_4), \tag{A-1}$$

$$\Gamma^{qq}_{\eta\eta'} = \frac{2a+b}{120\,a^{3/2}}(\gamma_2+\gamma_6)+\frac{1}{40\sqrt{c}}(\gamma_1+\gamma_5) + \frac{2a-5b+3c}{120\,d^{3/2}}(\gamma_3+\gamma_4)+\frac{e-f}{60\,a^{3/2}}+\frac{e-g}{60\,d^{3/2}}, \tag{A-2}$$

$$\Gamma^{qq}_{\eta\xi} = \frac{1}{120\sqrt{c}}\gamma_1+\frac{1}{120\sqrt{a}}\gamma_2+\frac{2a-3b+c}{120\,d^{3/2}}\gamma_3 + \frac{a-3b+2c}{120\,d^{3/2}}\gamma_4+\frac{3b+2c}{120\,c^{3/2}}\gamma_5+\frac{2a+3b}{120\,a^{3/2}}\gamma_6 + \frac{e-f}{40\,a^{3/2}}+\frac{g-f}{40\,c^{3/2}}, \tag{A-3}$$

$$\Gamma_{\eta'}^{qq} = \frac{1}{24\sqrt{c}}\gamma_1 + \frac{1}{24\sqrt{a}}\gamma_2 + \frac{1}{24\sqrt{d}}\gamma_3 + \frac{a-3b+2c}{24d^{3/2}}\gamma_4 + \frac{1}{12\sqrt{c}}\gamma_5 + \frac{a+b}{24a^{3/2}}\gamma_6 + \frac{e-f}{24a^{3/2}} + \frac{e-g}{24d^{3/2}} \quad \text{(A-4)}$$

where

$$\gamma_1 = \ln(f+b) - \ln(g+i), \quad \text{(A-5)}$$

$$\gamma_2 = \ln(e+h) - \ln(f-b), \quad \text{(A-6)}$$

$$\gamma_3 = \ln(e+h) - \ln(g+i), \quad \text{(A-7)}$$

$$\gamma_4 = \ln(g-i) - \ln(e-h), \quad \text{(A-8)}$$

$$\gamma_5 = \ln(g-i) - \ln(f-b), \quad \text{(A-9)}$$

$$\gamma_6 = \ln(f+b) - \ln(e-h), \quad \text{(A-10)}$$

$$a = (\mathbf{r}_3 - \mathbf{r}_1)\cdot(\mathbf{r}_3 - \mathbf{r}_1), \quad \text{(A-11)}$$

$$b = (\mathbf{r}_3 - \mathbf{r}_1)\cdot(\mathbf{r}_3 - \mathbf{r}_2), \quad \text{(A-12)}$$

$$c = (\mathbf{r}_3 - \mathbf{r}_2)\cdot(\mathbf{r}_3 - \mathbf{r}_2), \quad \text{(A-13)}$$

$$d = a - 2b + c, \quad \text{(A-14)}$$

$$e = \sqrt{a\,d}, \quad \text{(A-15)}$$

$$f = \sqrt{a\,c}, \quad \text{(A-16)}$$

$$g = \sqrt{c\,d}, \quad \text{(A-17)}$$

$$h = a - b, \quad \text{(A-18)}$$

$$i = b - c. \quad \text{(A-19)}$$

It can be shown that

$$\Gamma_{\xi\xi'}^{qq} = \Gamma_{\eta\eta'}^{qq}, \quad \text{(A-20)}$$

$$\Gamma_{\eta\xi'}^{qq} = \Gamma_{\xi\eta'}^{qq}, \quad \text{(A-21)}$$

$$\Gamma_{\xi'}^{qq} = \Gamma_{\eta'}^{qq} = \Gamma_{\xi}^{qq} = \Gamma_{\eta}^{qq}. \quad \text{(A-22)}$$

REFERENCES

[1] G. Miano and F. Villone, "A surface integral formulation of Maxwell equations for topologically complex conducting domains," *IEEE Trans. Antennas Propagat.*, vol. 53, no. 12, pp. 4001 - 4014, Dec. 2005.

[2] D. B. Davidson, "Computational Electromagnetics for RF and Microwave Engineering," Cambridge University, 2005.

[3] V. I. Okhmatovski, J. D. Morsey and A. C. Cangellaris, "Loop-tree implementation of adaptive integral method (AIM) for numerically-stable, broadband, fast electromagnetic modeling," *IEEE Trans. Antennas Propagat.*, vol. 52, pp. 2130 - 2140, 2004.

[4] Y. Wang, D. Gope, V. Jandhyala, and C. J. R. Shi, "Generalized Kirchoff's current and voltage law formulation for coupled circuit-electromagnetic simulation with surface integral equations," *IEEE Trans. Microwave Theory Tech.*, vol. 52, pp. 1673 - 1682, 2004.

[5] Z. Wang, J. Volakis, K. Saitou, and K. Kurabayashi, "Comparison of semi-analytic formulations and Gaussian-quadrature rules for quasi-static double-surafce potential integrals," *IEEE Antennas Propagat. Magazine*, vol. 45, no. 6, pp. 96 – 102, Dec. 2003.

[6] J. S. Zhao and W. C. Chew, "Integral equation solution of Maxwell's equations from zero frequency to microwave frequency," *IEEE Trans. Antennas Propagat.*, vol. 48, pp. 1635 - 1645, 2000.

[7] J. Lee, R. Lee, and R. J. Burkholder, "Loop star basis functions and a robust preconditioner for EFIE scattering problems," *IEEE Trans. Microwave Theory Tech.*, vol. 51, pp. 1855 – 1863, Aug. 2003.

[8] S. M. Rao, D. R. Wilton, and A. W. Glisson, "Electromagnetic scattering by surfaces of arbitrary shape," *IEEE Trans. Antennas Propagat.*, vol. 30, no. 3, pp. 409 - 418, May 1982.

[9] D. J. Taylor, "Accurate and efficient numerical integration of weakly singular integrals in Galerkin EFIE solutions," *IEEE Trans. Antennas Propagat.*, vol. 51, no. 7, pp. 1630 - 1637, July 2003.

[10] P. Acrioni, M. Bressan, and L. Perregrini, "On the evaluation of the double surface integrals arising in the application of the boundary integral method to 3-D problems," *IEEE Trans. Microwave Theory Tech.*, vol. 45, no 3, pp. 436 - 439, March 1997.

[11] T. F. Eibert and V. Hansen, "On the calculation of potential integrals for linear source distributions on triangular domains," *IEEE Trans. Antennas Propagat.*, vol. 43, no. 12, pp. 1499 - 1502, Dec. 1995.

[12] K. F. A. Hussein, "Analysis of conical equiangular spiral antenna using EFIE technique," *National Radio Science NRCS'2004*, B21, Cairo, Egypt, pp. 1-11, March 2004.

[13] A. A. Lestari, A. G. Yarovoky, and L. P. Ligthart, "Numerical analysis of transient antennas," http://www.tudelft.nl/live/binaries/33dc3ad6-3e8a-4bdd-8456-1f3d10b39c8c/doc/Lestari_turin.PDF.

[14] S. Watanabe and M. Taki, "An improved FDTD model for the feeding gap of a thin-wire antenna," *IEEE Microwave Guided Wave Lett.*, vol. 8, no. 4, pp. 152 – 154, April 1998.

[15] Y. Cho, D. Choi, and S. Park, "FDTD analysis of bow-tie antenna by incorporating approximated static field solutions," *IEEE Antennas Wireless Propagat. Lett.*, vol. 3, pp. 176 - 179, 2004.

[16] A. J. Kerkhoff, R. L. Rogers, and H.Ling, "Design and analysis of planar monopole antennas using a genetic algorithm approach," *IEEE Trans. Antennas Propagat.*, vol. 52, no. 10, pp. 2709 - 2718, Oct. 2004.

[17] K. Lee, C. Chen, F. L. Teixeira, and R. Lee, "Modeling and investigation of a geometrically complex UWB GPR antenna using FDTD," *IEEE Trans. Antennas Propagat.*, vol. 52, no. 8, pp. 1983 - 1991, Aug. 2004.

[18] A. A. Lestari, A. G. Yarovoky, and L. P. Ligthart, "An efficient ultra wideband bow-tie antenna," http://www.tudelft.nl/live/binaries/33dc3ad6-3e8a-4bdd-8456-1f3d10b39c8c/doc/Lestari_london.PDF.

[19] A. A. Lestari, A. G. Yarovoky, and L. P. Ligthart, "Ground influence on the input impedance of transient dipole and bow-tie antennas," *IEEE Trans. Antennas Propagat.*, vol. 52, no. 8, pp. 1970 - 1975, Aug. 2004.

[20] F. J. Gonzalez and G. D. Boreman, "Comparison of dipole, bowtie, spiral and log-periodic IR antennas," *Elsevier Infrared Physics Technology*, vol. 46, pp. 418 – 428, 2005.

[21] D. Uduwawala, M. Norgren, and P. Fuks, "A complete FDTD simulation of a real GPR antenna system operating above lossy and dispersive grounds," PIER, vol. 50, pp. 209 – 229, 2005.

[22] J. Thaysen, K. B. Jakobsen, and J. Apple-Hansen, "A logarithmic spiral antenna for 0.4 to 3.8 GHz," *Applied Microwave and Wireless*, http://www.ctsystemes.com/zeland/public /pg32. pdf.

[23] L. Sevgi and G. Cakir, "A broadband array of Archimedean spiral antennas for wireless applications," *Microwave Optical Tech. Lett.*, vol. 48, no. 1, pp. 195 - 200, Jan. 2006.

[24] P. Piska, "Log-spiral antenna from 2 to 40 GHz with impedance matching," http://www. ctsystemes.com/zeland/publi/j2004_266.pdf, Jan. 2004.

[25] R. Sivan-Sussman, "Various modes of the equiangular spiral antenna," *IEEE Trans. Antennas Propagat.*, vol. 11, pp. 533 – 539, 1963.

[26] D. Sievers, T. F. Eibert, and V. Hansen, "Correction to on the calculation of potential integrals for linear source distributions on triangular domains," *IEEE Trans. Antennas Propagat.*, vol. 53, pp. 3113, 2005.

Khalid F. A. Hussein was born in Hawamdiah, Giza, Egypt in 1968. He received the BSc., MSc., and PhD. from Cairo University, Faculty of Engineering, Electronics and Electrical Communications Department in 1990, 1995, and 2001, respectively. He is interested in the research fields of antennas, electromagnetic scattering, GPR, and biological effects of electromagnetic radiation.